

Large, Negative Magnetoresistance in an Oleic Acid-Coated Fe₃O₄ Nanocrystal Self-Assembled Film

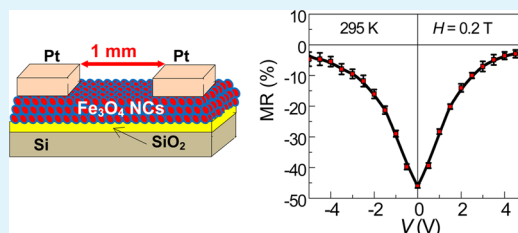
Shigemi Kohiki,^{*,†} Tomoki Kinoshita,[†] Koichiro Nara,[†] Kotone Akiyama-Hasegawa,[§] and Masanori Mitome[§]

[†]Department of Materials Science, Kyushu Institute of Technology, 1-1 Sensui, Tobata, Kitakyushu, Fukuoka 804-8550, Japan

[§]International Center for Materials Nanoarchitectonics, National Institute for Materials Science, 1-1 Namiki, Tsukuba, Ibaraki 305-0044, Japan

ABSTRACT: An oleic acid-coated Fe₃O₄ nanocrystal self-assembled film was fabricated via drop casting of colloidal particles on a SiO₂/Si substrate. The film exhibited bifurcation of the zero-field-cooled and field-cooled magnetizations around 250 K. The nonlinear current-voltage (*I*–*V*) characteristics between the source and drain electrodes in both zero and non-zero magnetic fields (*H*) were observed above and below the bifurcation temperature. A large negative magnetoresistance (MR ≈ –60%) was achieved at 200 K and *H* = 1 T. Even at 295 K and 0.2 T, the negative MR (~ –50%) persisted. A Fowler–Nordheim plot and power-law scaling of the *I*–*V* characteristics revealed that the current flows through two-dimensional (2D) percolated electron tunneling paths. The enlargement of MR can be attributed to spin-dependent electron tunneling between magnetically coupled Fe₃O₄ nanocrystals self-assembled in 2D ordered arrays.

KEYWORDS: negative magnetoresistance, Fe₃O₄ nanocrystals, oleic acid, self-assembly, two-dimensional networks



INTRODUCTION

Magnetoresistance (MR) in half-metals has been the focus of basic and applied studies for spintronics device applications. Half-metals are conductors with a continuous energy band at the Fermi level for one spin channel, and insulators with an energy gap at the Fermi level for another spin channel. The half-metal Fe₃O₄ is suitable for spintronic devices operating above room temperature (RT) because it has fully spin-polarized (*P* = 100%) carriers up to its Curie temperature (~840 K).^{1,2} Thus, it should be possible to employ the large, negative MR of an oleic acid (OA)-coated Fe₃O₄ nanocrystal (NC) self-assembled film³ to switch the current between the source and drain electrodes of a two-terminal spin device, and the large MR should bring about very high performance.

In multiple junction systems consisting of Fe₃O₄ NCs weakly electrically contacting one another via thin, insulating OA barriers, the MR is defined as $MR = (R_H - R_0)/R_0$, where *R_H* and *R₀* are the differential resistance (*R* = *dV/dI*) for nonlinear source-drain current and bias-voltage (*I*–*V*) characteristics in non-zero (*H* ≠ 0) and zero (*H* = 0) magnetic fields, respectively. Each Fe₃O₄ NC possesses spontaneous magnetization along the [111] easy axis. When the angle between the magnetization of adjacent Fe₃O₄ NCs in three-dimensional (3D) systems is denoted by *θ*, the relative magnetization of the system *m* relates to *θ* as $m^2 = \langle \cos \theta \rangle$.⁴ Application of a sufficiently strong field (*H* ≠ 0) entirely changes the configuration of magnetizations in the system to be in parallel (*θ* = 0), and then maximizes the spin-dependent electron tunneling probability between the NCs by fulfilling the condition *m* = 1. When the tunneling resistivity is varied

from high to low, the sign of MR becomes negative.⁵ Since MR is connected to *P* and *m* by $MR \equiv P^2 m^2 / (1 + P^2 m^2)$,⁴ then both *P* = 100% and *m* = 1 are required to maximize MR (= –50%) in 3D systems.

Even at RT, *P* = 100% is theoretically expected for Fe₃O₄. Poddar et al. reported an MR of –300% at 110 K and –125% above 150 K in 0.25 T for OA-encapsulated Fe₃O₄ nanoparticles.⁶ Zeng et al. reported an MR = –35% at 60 K in 3.5 T for organic surfactant-covered Fe₃O₄ nanoparticles with a superparamagnetic blocking temperature (*T_b*) of 40 K.⁷ Wang et al. reported an MR = –40.9% at 110 K in 14 T for a 3D network of spherical Fe₃O₄ particles dispersed in polystyrene.⁸ Wang et al. reported an MR = –10.8% at 1 T and –17% at 8 T for SiO₂-coated nanospheres of Fe₃O₄.⁹ Kant et al. reported an MR at 100 K of –11.5% and –5.8% in 1 T for Fe₃O₄ nanoparticles coated with thin SiO₂ and ZnO layers, respectively.¹⁰ They reported a *T_b* = 200 K for the samples. Wang et al.¹¹ reported an MR in 5 T of –21% at 130 K and –13% at 280 K for Fe₃O₄ nanoparticles dispersed in hexabromobenzene. Wang et al.¹² reported an MR in 0.58 T of –17% at 115 K and –7% at RT for OA-covered Fe₃O₄ nanoparticles. They also reported that an interparticle separation (*s*) of ~4 nm by surface-coated OA molecules enhanced the MR by more than two times over uncoated Fe₃O₄ nanoparticles. The rather large MR values below 130 K for the Fe₃O₄ nanoparticle systems reflect an increase in the

Received: July 3, 2013

Accepted: October 29, 2013

Published: October 29, 2013

resistivity due to the Verwey transition in the Fe_3O_4 crystal lattice.¹³ Taub et al. reported an MR of -25% at 250 K in 0.8 T for OA-coated Fe_3O_4 nanoparticles with a T_b of $\sim 220\text{ K}$.¹⁴ They also reported the temperature dependence of MR exhibiting a maximum around T_b . However, the value of MR, even at T_b , was far from -50% . As mentioned above, the rather large MR values for superparamagnetic 3D systems reflect the intra-particle Verwey transition.

Previously, we reported that two-dimensional (2D) hexagonal networks of OA- $\text{Fe}_{2.3}\text{Mn}_{0.5}\text{O}_4$ NCs exhibit both a spin glass (SG) transition around 150 K and a large MR $\approx -40\%$ at 200 K in $H = 0.5\text{ T}$.³ Enlargement of MR can be achieved by building 2D ordered arrays of the NCs, in which geometrically frustrated networks of collinear magnetic moments increase R_0 and decrease R_H in intergranular tunneling of spin-polarized electrons. The spontaneous self-assembly phenomenon is commonly used to control the arrangement of the NCs into hexagonally ordered arrays.^{15,16} Oleic acid, $\text{CH}_3(\text{CH}_2)_7\text{CH}=\text{CH}(\text{CH}_2)_7\text{COOH}$, is an unsaturated carboxylic acid with a cis-double-bond "kink" in the middle of its C_{18} tail. The polar head group chemisorbs to the hydrophilic surface of nanoparticles, and steric repulsion of the long chain prevents the NCs from agglomerating.¹⁷ Since OA-NCs are hydrophobic, the slow drying of a hexane colloidal suspension dropped onto a substrate results in a self-assembled film with hexagonally aligned NC arrays. Furthermore, hydrophobization by OA is highly advantageous in preventing the lowering of observed spin-polarization due to surface oxidation of Fe_3O_4 NCs.¹⁸

As a foundation for a high-performance spin device, the MR of a drop-cast OA- Fe_3O_4 NC self-assembled film was examined. Nonlinear I - V characteristics were observed above 200 K in $H < 1\text{ T}$. At 200 K , the MR of the film reached -54% at 0.5 T and -58% at 1 T . Even at 295 K , the MR value of the film remained at -46% in 0.2 T . The observed MR values at 200 K are larger than the maximum possible (-50%) for 3D systems with $P = 100\%$ and $m = 1$. A Fowler-Nordheim plot and power-law scaling of the I - V curves clarified that the current flows through 2D percolated electron tunneling paths formed in the film. The MR larger than -50% was achieved by spin-dependent electron tunneling between magnetically-coupled Fe_3O_4 nanocrystals self-assembled in 2D ordered arrays.

EXPERIMENTAL SECTION

Synthesis of Fe_3O_4 NCs and Fabrication of the NC Self-assembled Film. Fe_3O_4 NCs were synthesized from $\text{Fe}(\text{acac})_3$ in a solution of dibenzylether mixed with OA.²¹ $\text{Fe}(\text{acac})_3$, dibenzylether, and OA, in a molar ratio of 6:157:12, were mixed with vigorous stirring for an hour at RT, and then the mixture was refluxed at 573 K for half an hour. After cooling to RT, the NCs were precipitated from the crude solution by adding a mixture of toluene/hexane (1:1) followed by centrifugation. The precipitated NCs were washed with anhydrous chloroform. The Fe_3O_4 NCs were dispersed in a weak alkaline ($\text{pH} = 10.4$) aqueous solution. After stirring for 10 minutes, additional OA (molar ratio of $[\text{Fe}]/[\text{C}_{18}\text{H}_{34}\text{O}_2] = 1:42$) was added to the solution with vigorous stirring. After the mixture was stirred for 20 minutes, 1 N HCl aqueous solution was added to neutralize the solution. After removal of the transparent solvent, the precipitated OA- Fe_3O_4 NCs were dispersed in hexane. The OA- Fe_3O_4 NCs were used without post-preparative size selection for fabrication of the self-assembled film. The colloidal suspensions in hexane were dropped onto a SiO_2/Si substrate, and then dried at 573 K for half an hour at 100 Pa to yield the OA- Fe_3O_4 NC self-assembled film.

Structural, Magnetic, and Magnetoelectric Characterization. The crystal structures of the NCs and the NC self-assembled film were confirmed via X-ray diffraction (XRD) using a Rigaku CN2013 X-ray

diffractometer with $\text{Cu K}\alpha$ radiation. The size and shape of the NCs were examined using a JEOL JEM-3100FEF transmission electron microscope (TEM) operated at an electron acceleration voltage of 300 kV .

Magnetic and magnetoelectric characterization was carried out using a superconducting quantum interference device (SQUID) magnetometer (Quantum Design, MPMS-5S). For the temperature dependence of the DC magnetization (M - T) measurements, the sample was cooled from RT to 5 K in $H = 0$, and then $H = 0.03\text{ T}$ was applied. The zero-field-cooled (ZFC) magnetization was recorded with rising temperature to 300 K . After the ZFC measurement, the sample was again cooled to 5 K in $H = 0.03\text{ T}$, and then the field-cooled (FC) magnetization was recorded with rising temperature to 300 K . Both the real (χ') and imaginary (χ'') parts of the complex susceptibility were measured from 5 to 300 K upon warming in an AC field (H_{AC}) of 3.8 G at a frequency (f) of 1 - 100 Hz . For the magnetoelectric measurements, Pt electrodes were bonded via gold wires to the MPMS-5S system. H was applied parallel to I between the source and drain electrodes spaced 1 mm apart. For each I - V measurement, the $H = 0$ character was measured first, followed by the $H \neq 0$.

RESULTS AND DISCUSSION

The as-synthesized NCs demonstrate an XRD pattern attributable to the cubic Fe_3O_4 crystal lattice ($a = 0.84\text{ nm}$) with space group $Fd\bar{3}m$ (JCPDS 19-0629), as shown in Figure 1a. The crystallite size, estimated from the half-width of the

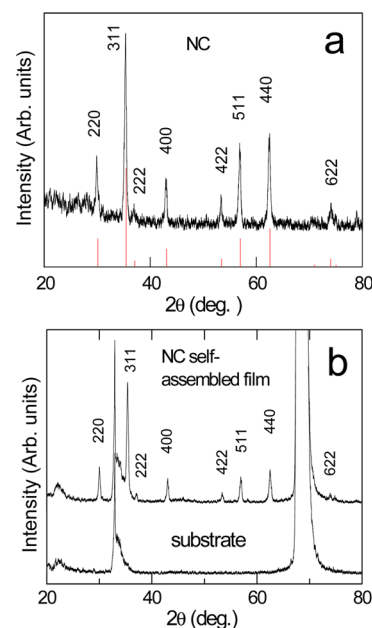


Figure 1. XRD pattern of as-synthesized NCs with peaks from the JCPDS 19-0629 (red bars) of Fe_3O_4 (a). XRD patterns of the OA- Fe_3O_4 NC/ SiO_2/Si sample and an SiO_2/Si substrate (b).

(511) reflection peak using Scherer's equation, amounts to $\sim 50\text{ nm}$. The XRD patterns shown in Figure 1b indicate that the sample consists of Fe_3O_4 NCs and a SiO_2/Si substrate.

As shown in the upper panel of Figure 2, ordered arrays of NCs having a lateral size (d) of $\sim 50\text{ nm}$ were built in the self-assembled film. Rows of NCs appear in the film, accompanied with disorder as reported in ref 22 and demonstrated a preferred orientation to some extent, as shown in the lower panel of Figure 2. In a $300 \times 300\text{ nm}^2$ region, 36 NCs were typically counted, so the mean area occupied by a single NC (A_{NC}) amounts to 2500 nm^2 . Assuming a hexagonal arrangement of the NCs,³ the equation $A_{\text{NC}} = (\sqrt{3}/2)(d+s)^2$ gives an s

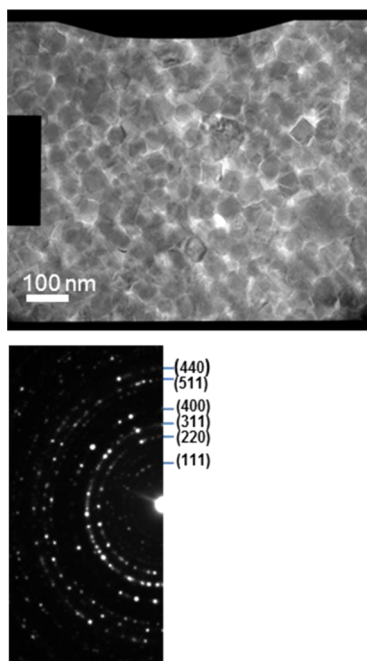


Figure 2. Low-magnification cross-sectional TEM image (upper panel) and selected area electron diffraction pattern (lower panel) of OA-Fe₃O₄ NC self-assembled film.

of ~ 3 nm, which is in good agreement with that reported in ref 23. The upper panel of Figure 3 shows that the entire NC is a

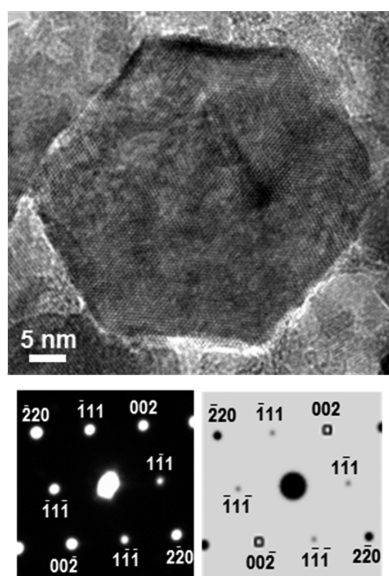


Figure 3. High-resolution TEM image of a single grain (upper panel), nano beam diffraction pattern from the grain (lower left), and model of the diffraction pattern from an Fe₃O₄ crystal with the incident beam direction along the [110] axis (lower right).

single crystal without stacking faults or twins. The distinctive spots of a nano beam diffraction pattern (Figure 3, lower left panel) from the NC can be simulated well by a centrosymmetric Fe₃O₄ crystal lattice (JCPDS 19-0629) with the incident beam direction along the [110] axis, as shown in the lower right panel. Thus, the Fe₃O₄ NCs composing the self-assembled film are single crystals.

In the field-dependent magnetization ($M-H$) at 200 K, the NCs exhibited a nearly-saturated sigmoidal curve above $H \approx 0.5$ T with $M = 1.3 \mu_B/\text{Fe}$, which is equivalent to the spontaneous magnetization of Fe₃O₄. However, the sample possessed a nearly-saturated M of $0.5 \mu_B/\text{Fe}$ above $H \approx 0.2$ T, as shown in Figure 4a. Consequently, the mass percentage of Fe₃O₄ in the sample amounts to approximately 39%.

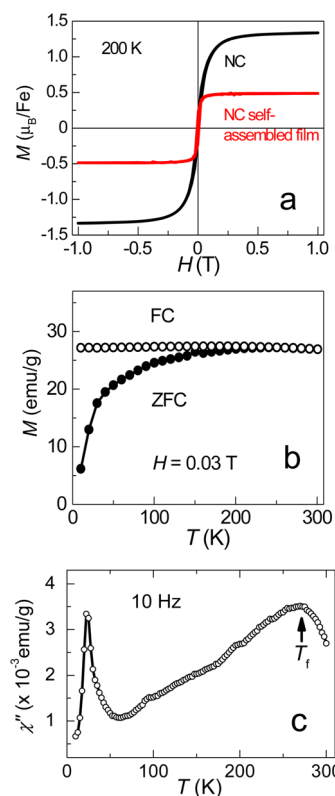


Figure 4. $M-H$ curves of the NCs and the sample (red line) at 200 K (a). FC and ZFC $M-T$ curves of the sample at $H = 0.03$ T (b). $\chi''-T$ curve for the ZFC sample with an f of 10 Hz (c).

As shown in Figure 4b, the sample demonstrated bifurcation of the FC and ZFC magnetizations below 250 K. The FC magnetization remained almost constant below 250 K, whereas the ZFC fell off gradually with decreasing temperature. Such a cooling history-dependence of the DC magnetization suggests an SG transition around 250 K for the sample. With regard to the $\chi'-T$ and $\chi''-T$ AC characteristics of the ZFC sample, χ' decreased almost linearly with decreasing temperature from 288 to 30 K (not shown), while χ'' showed a broad peak around 270 K and a narrow peak around 20 K, as shown in Figure 4c. The χ'' anomaly at 20 K is an indication of the supersinglass transition in each isolated Fe₃O₄ NC,²⁴ while the one at 270 K (the freezing temperature, T_f) peculiar to the film is indicative of the slow dynamics common in self-assembled OA-Fe₃O₄ NCs.^{25,26} Such a high T_f reflects the strong dipolar interactions among the magnetic moments of the Fe₃O₄ NCs isolated (~ 3 nm apart) by OA molecules adsorbed on their surfaces, and affects the MR, even at RT. Below T_f the sample is in a frustrated magnetic state. With increasing temperature, the frozen magnetic moments thaw progressively. Even at RT, near T_f the magnetic moments are still frozen partly, switching randomly. The randomly-oriented magnetic moments of the NCs in percolating current paths give rise to an enlarged R_0 . An

applied field ($H \neq 0$) rotates the magnetic moments of the NCs to mutual alignment ($m = 1$), and enlarges the spin-polarized tunneling rate for multiple inter-particle junctions, which then results in a largely enhanced negative MR for the sample.

At 200 K, the sample demonstrated the nonlinear I - V characteristics typical of an intergranular tunneling conductance mechanism,²⁷ as shown in Figure 5a. $R (= dV/dI)$ in $H = 0$ and

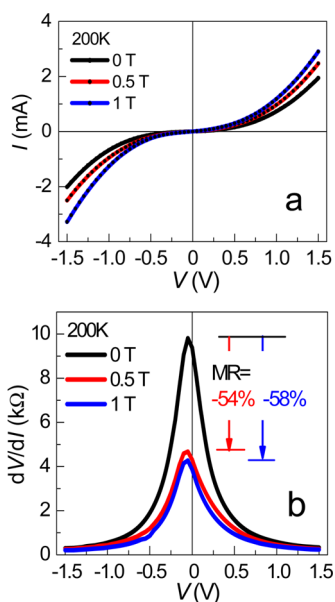


Figure 5. I - V characteristics of the sample measured at 200 K in $H = 0, 0.5,$ and 1 T (a). dV/dI versus V plot of the I - V curves at 200 K (b).

$H \neq 0$ were high and low, respectively, as seen in Figure 5b. An applied field ($H = 0.5$ T) aligned the magnetic moments of the Fe_3O_4 NCs parallel to each other, and enlarged the electron tunneling probability between the spin-polarized conduction bands of adjacent Fe_3O_4 NCs. The dV/dI curves peaked around $V = 0$ and fell off rapidly with increasing V . The (dV/dI) - V characteristic of a single interparticle tunneling junction is assumed to be proportional to the density of occupied states of the Fe_3O_4 NC on the source-electrode side, and that of empty states on the drain-electrode side. Electron tunneling at different V probes different energy ranges of the density of states above the Fermi level of the Fe_3O_4 NC on the drain-electrode side. Therefore, the ≈ 1 V width of the dV/dI peak may be the result of the conduction band of the Fe_3O_4 NCs with a width of ~ 0.5 eV. At 200 K, an MR of -54% was observed in 0.5 T, and -58% in 1 T. Such a saturation in MR above $H = 0.5$ T is consistent with that in M above $H \approx 0.2$ T. The observed MR below T_f is larger than the value of -50% expected for a 3D Fe_3O_4 NC system with $P = 100\%$ and $m = 1$,⁴ however an MR $\approx -120\%$ at 200 K in 0.25 T was reported by Poddar et al.⁶ for arrays of OA- Fe_3O_4 NCs.

As shown in Figure 6a, the I - V characteristics of the sample were also measured at 295 K under an H perpendicular to I . It is well known that there is no geometrical effect on MR for granular systems. Tripathy et al.²⁸ reported that, for an Fe_3O_4 - Al_2O_3 granular system, the MR measured with H perpendicular to I was identical to that measured with H parallel to I . An anisotropic effect is absent in the MR of granular systems. Even at 295 K, the nonlinearity in the I - V characteristics was preserved. As shown in Figure 6b, the larger dV/dI in 0 T

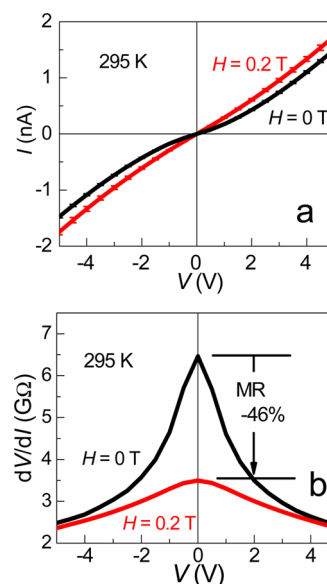


Figure 6. I - V characteristics of the sample measured at 295 K in $H = 0$ and 0.2 T (a). dV/dI versus V plot of the I - V curves at 295 K (b).

compared to that in 0.2 T resulted in a negative MR of -46% . Increasing the temperature should lessen the degree of spin polarization near the Fermi level, although a large negative MR was still retained at RT. Assuming $m = 1$, even in $H = 0.2$ T, the MR = -46% corresponds to $P = 93\%$ at RT, which seems to be consistent with the half-metallic nature of Fe_3O_4 .

An intergranular tunneling conductance mechanism for the MR of the sample above 150 K is supported by the linear relationship in the $\ln R_0 (= dV|_{V=0}/dI)$ versus $T^{-1/2}$ plot shown in Figure 7a. Such a $T^{-1/2}$ dependence denotes that the MR of the sample is dominated by direct electron tunneling between adjacent Fe_3O_4 NCs in current paths. A Fowler-Nordheim plot of the I - V curves at 200 and 295 K, derived from the $V = 0$ limit equation $\ln(I/V^2) \propto \ln(1/V) - [2s(2m_e)^{1/2}/\hbar]\Phi^{1/2}$, where s is the barrier thickness, m_e is the effective mass of the electron, and Φ is the barrier height for electron tunneling,²⁹ are shown in Figure 7b and 7c, respectively. While the plot at 200 K demonstrates an inflection point at ~ 1.3 V corresponding to a transition from direct tunneling to Fowler-Nordheim tunneling, the plot at 295 K shows only logarithmic growth toward the zero V limit. The plot sustains the thesis that even at RT, the observed MR is dominated by direct electron tunneling across the OA layer between two adjacent Fe_3O_4 NCs.

The observed nonlinear I - V characteristics suggest that the sample is highly insulating below $|V| = 0.5$ V since the tunnel current is blocked due to local charging of the NCs by a single electron. Above the Coulomb blockade threshold ($V_T = 0.5$ V), electron tunneling paths between the source and drain electrodes are opened, and the tunnel current starts to flow via the NCs, not via thermally-activated electron hopping, even at RT, as mentioned above. Since the observed MR (over -50%) cannot be predicted by 3D NC systems,⁴ the dimensionality of the spin-dependent electron tunneling paths was examined via power-law scaling with the equation $I \approx (V - V_T)^{\xi}$ ¹⁹ based on a Coulomb blockade model.²⁰ The experimental I - V characteristics beyond V_T were fitted well with the critical exponents $\xi \approx 1.6$ - 1.7 , as shown in Figure 8. The critical exponents ξ for 1D and 2D NC arrays have been

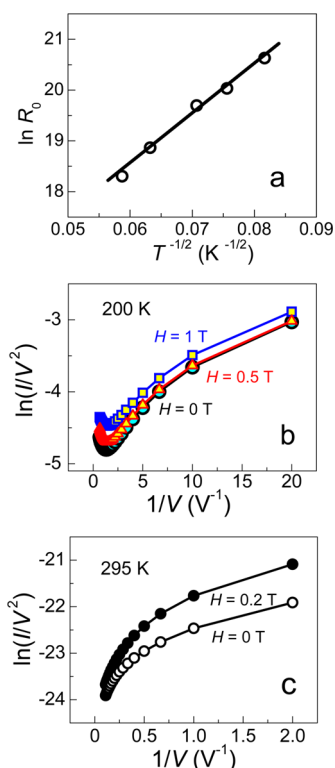


Figure 7. $\ln R_0$ versus $T^{-1/2}$ plot for the sample with a line of best fit (a). Fowler–Nordheim plot of the I – V curves measured at 200 (b) and 295 K (c).

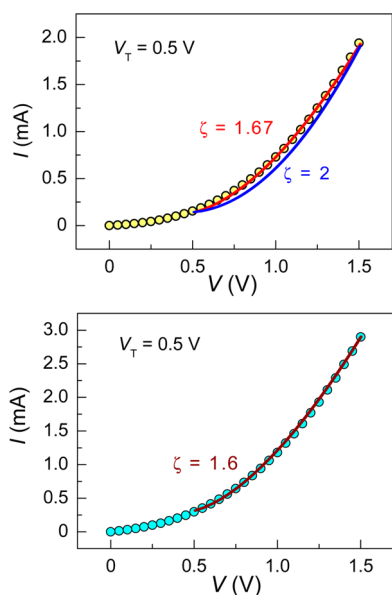


Figure 8. Fitting of the experimental I – V curves at 200 K in $H = 0$ (upper panel) and 1 T (lower panel) to estimate the ξ value.

analytically determined to be 1 and $5/3$, respectively.²⁰ There is excellent agreement of the experimental I – V characteristics with the scaling law (universal ξ of $5/3$), meaning 2D percolated electron tunneling paths are opened above V_T . V_T is amplified by over tenfold in 2D NC arrays because of single electrons charging at multiple sites in the percolation path.²⁰ It has been reported that below V_T , sequential tunneling is superseded by coherent tunneling, which is sensitive to the relative orientation of magnetization between the NCs.³⁰ The

Coulomb blockade MR is theoretically expected to reach over 1000% at RT when adjacent NCs couple magnetically.³¹ The present MR ($\sim -60\%$) at 200 K in 1 T around $V \approx 0$ V is due to spin-dependent electron tunneling between magnetically coupled OA- Fe_3O_4 NCs in self-assembled 2D arrays.

CONCLUSION

A large, negative MR brings about high performance in a normally OFF-type spin-dependent current switch. In an OA- Fe_3O_4 NC self-assembled film exhibiting an SG transition with $T_f \approx 270$ K, nonlinear I – V characteristics were observed, resulting in an MR = -54% in 0.5 T and -58% in 1 T at 200 K, and -46% in 0.2 T at 295 K. A spin-polarized current flowed through 2D percolated electron tunneling paths. The MR observed is larger than the maximum for 3D systems with both $P = 100\%$ and $m = 1$, and is attributed to an enlarged probability of spin-dependent electron tunneling in the Coulomb blockade region between magnetically coupled Fe_3O_4 NCs self-assembled in 2D ordered arrays.

AUTHOR INFORMATION

Corresponding Author

*E-mail: kohiki@che.kyutech.ac.jp.

Notes

The authors declare no competing financial interest.

ACKNOWLEDGMENTS

S.K. thanks the support of a Yoshida Research Grant for this work. This work was partly supported by the “Nanotechnology Platform Project” of the Ministry of Education, Culture, Sports, Science and Technology, Japan.

REFERENCES

- (1) Yanase, A.; Siratori, K. *J. Phys. Soc. Jpn.* **1984**, *53*, 312–317.
- (2) Zhang, Z.; Satpathy, S. *Phys. Rev. B* **1991**, *44*, 13319–13331.
- (3) Kohiki, S.; Okada, K.; Mitome, M.; Kohno, A.; Kinoshita, T.; Iyama, K.; Tsunawaki, F.; Deguchi, H. *ACS Appl. Mater. Interfaces* **2011**, *3*, 3589–3593.
- (4) Inoue, J.; Maekawa, S. *Phys. Rev. B* **1996**, *53*, R11927–R11929.
- (5) Julliere, M. *Phys. Lett.* **1975**, *54A*, 225–226.
- (6) Poddar, P.; Fried, T.; Markovich, G. *Phys. Rev. B* **2002**, *65*, No. 172405.
- (7) Zeng, H.; Black, C. T.; Sandstrom, R. L.; Rice, P. M.; Murray, C. B.; Sun, S. *Phys. Rev. B* **2006**, *73*, 020402(R).
- (8) Wang, W.; Yu, M.; Batzill, M.; He, J.; Diebold, U.; Tang, J. *Phys. Rev. B* **2006**, *73*, No. 134412.
- (9) Wang, J.; Shi, J.; Tian, D.; Deng, H.; Li, Y.; Song, P.; Chen, C. *Appl. Phys. Lett.* **2007**, *90*, No. 213106.
- (10) Kant, K. M.; Sethupathi, K.; Rao, M. S. R. *J. Appl. Phys.* **2008**, *103*, No. 07F318.
- (11) Wang, W.; He, J.; Tang, J. *J. Appl. Phys.* **2009**, *105*, No. 07B105.
- (12) Wang, S.; Yue, F. J.; Wu, D.; Zhang, F. M.; Zhong, W.; Du, Y. *W. Appl. Phys. Lett.* **2009**, *94*, No. 012507.
- (13) Ziese, M.; Blythe, H. J. *J. Phys.: Condens. Matter* **2000**, *12*, 13–28.
- (14) Taub, N.; Tsukernik, A.; Markovich, G. *J. Magn. Magn. Mater.* **2009**, *321*, 1933–1938.
- (15) Murray, C. B.; Kagan, C. R.; Bawendi, M. G. *Ann. Rev. Mater. Sci.* **2000**, *30*, 545–610.
- (16) Prasad, B. L. V.; Sorensen, C. M.; Klabunde, K. J. *Chem. Soc. Rev.* **2008**, *37*, 1871–1883.
- (17) Tadmor, R.; Rosensweig, R. E.; Frey, J.; Klein, J. *Langmuir* **2000**, *16*, 9117–9120.
- (18) Rybchenko, S. I.; Fujishiro, Y.; Takagi, Y.; Awano, M. *Phys. Rev. B* **2005**, *72*, No. 054424.

- (19) Parthasarathy, R.; Lin, X. M.; Jaeger, H. M. *Phys. Rev. Lett.* **2001**, *87*, No. 186807.
- (20) Middleton, A. A.; Wingreen, N. S. *Phys. Rev. Lett.* **1993**, *71*, 3198–3201.
- (21) Kim, D.; Lee, N.; Park, M.; Kim, B. H.; An, K.; Hyeon, T. *J. Am. Chem. Soc.* **2009**, *131*, 454–455.
- (22) Zhang, L.; Wu, J.; Liao, H.; Hou, Y.; Gao, S. *Chem. Commun.* **2009**, 4378–4380.
- (23) Li, D.; Jiang, D.; Chen, M.; Xie, J.; Wu, Y.; Dang, S.; Zhang, J. *Mater. Lett.* **2010**, *64*, 2462–2464.
- (24) Suzuki, M.; Fullem, S. I.; Suzuki, I. S.; Wang, L.; Zhong, C.-J. *Phys. Rev. B* **2009**, *79*, No. 024418.
- (25) Doman, J. L.; Fiorani, D.; Trone, E. *Adv. Chem. Phys.* **1997**, *98*, 283–494.
- (26) Mydosh, J. A. *Spin Glasses: An Experimental Introduction*; Taylor & Francis: London, 1993.
- (27) Simmons, J. G. *J. Appl. Phys.* **1963**, *34*, 1793–1803.
- (28) Tripathy, D.; Adeyeye, A. O.; Shannigrahi, S. *Phys. Rev. B* **2007**, *76*, No. 174429.
- (29) Beebe, J. M.; Kim, B.; Gadzuk, J. W.; Frisbie, C. D.; Kushmerick, J. G. *Phys. Rev. Lett.* **2006**, *97*, No. 026801.
- (30) Takahashi, S.; Maekawa, S. *Phys. Rev. Lett.* **1998**, *80*, 1758–1761.
- (31) Zhang, X.-G.; Wen, Z. C.; Wei, H. X.; Han, X. F. *Phys. Rev. B* **2010**, *81*, No. 155122.